●●

The influence of Antarctic sea ice on glacial–interglacial CO_2 variations

Britton B. Stephens*† & Ralph F. Keeling*

* *Scripps Institution of Oceanography, University of California, San Diego, La Jolla, California 92093–0244, USA*

Ice-core measurements indicate that atmospheric CO_2 concentrations during glacial periods were consistently about 80 parts per million lower than during interglacial periods[1]. Previous explanations for this observation[2-9] have typically had difficulty accounting for either the estimated glacial O_2 concentrations in the deep sea, $^{13}C/^{12}C$ ratios in Antarctic surface waters, or the depth of calcite saturation; also lacking is an explanation for the strong link between atmospheric CO_2 and Antarctic air temperature[1]. There is growing evidence that the amount of deep water upwelling at low latitudes is significantly overestimated in most ocean general circulation models[10,11] and simpler box models previously used to investigate this problem. Here we use a box model with deep-water upwelling confined to south of 55 °S to investigate the glacial–interglacial linkages between Antarctic air temperature and atmospheric CO_2 variations. We suggest that low glacial atmospheric CO_2 levels might result from reduced deep-water ventilation associated with either year-round Antarctic sea-ice coverage, or wintertime coverage combined with ice-induced stratification during the summer. The model presented here reproduces 67 parts per million of the observed glacial–interglacial CO_2 difference, as a result of reduced air–sea gas exchange in the Antarctic region, and is generally consistent with the additional observational constraints.

Most theories for low glacial atmospheric CO_2 concentrations rely on one of two mechanisms: an increase in the strength of the biological pump as a result of changes in the supply or utilization of nutrients or light[2-6], or an increase in the ocean's alkalinity via coral reef dissolution[7] or carbonate sediment interactions[8,9]. Models that invoke biological pump changes are generally inconsistent with the magnitude and/or direction of glacial–interglacial changes in $^{13}C/^{12}C$ ratios and nutrients[12,13], and with the lack of widespread glacial deep-water anoxia. On the other hand, models invoking alkalinity changes predict large increases in the depth of the glacial lysocline which are not observed.

Our model is not based on productivity or alkalinity increases, but rather on changes in the rate of air–sea gas exchange as a result of increased sea-ice cover at high southern latitudes. By significantly limiting the sea-to-air CO_2 flux in the primary region for deep-water ventilation, expanded Antarctic sea ice during glacial times may trap relatively more carbon in the deep ocean, thereby reducing atmospheric CO_2 concentrations. This mechanism would increase the effectiveness of the biological pump at storing CO_2 in the deep ocean without actually increasing productivity, and thus would not necessarily require changes in nutrient concentrations or utilization efficiencies. Because dissolved O_2 equilibrates with the atmosphere more rapidly than CO_2, as a result of its lack of buffering chemistry, the limitation imposed by glacial sea ice would have a lesser effect on O_2 entering the deep ocean than on CO_2 leaving, and thus would not produce deep anoxia. Furthermore, increased Antarctic sea ice would not produce a large lysocline shift. Finally, the direct connections between Antarctic temperature and sea-ice cover provide a possible explanation for the observed synchrony between Antarctic temperature and atmospheric CO_2 concentrations during deglaciation[6].

Increases in Antarctic sea ice have been included in three-dimensional ocean model simulations, but their potential to significantly affect atmospheric CO_2 in these models may be limited by defects involving excessive low-latitude upwelling of deep water. Toggweiler and Samuels[10] have shown from ^{14}C comparisons, and Gnanadesikan and Toggweiler[11] from silica flux comparisons, that coarse-resolution ocean models all overestimate the amount of deep water upwelling across the main thermocline at low latitudes in the Indian and Pacific oceans. Previous box models used to explore palaeo-CO_2 controls[2–4,14,15] also overestimate deep-water upwelling at low latitudes. These models have from 15 to 40 Sv $(1 \text{ Sv} = 10^6 \text{ m}^3 \text{ s}^{-1})$ of upwelling directly from the deep to the warm surface box, which is much greater than the combined upper limit of ~ 7 Sv indicated by tracer and transect studies in the Pacific[10] and Indian[16] oceans.

To investigate the influence of Antarctic sea ice in the absence of low-latitude deep-water upwelling, we employ the biogeochemical ocean model shown in Fig. 1. The fundamental difference between this and other box models of the ocean carbon cycle is that deep waters only return to the surface south of the Antarctic Polar Front (APF), consistent with the "reconfigured conveyor" of Toggweiler and Samuels[10]. We divide the upper ocean into a warm, low-nutrient surface (S) box and a cooler, higher-nutrient thermocline (T) box. We also separate the upwelling that feeds the Antarctic Bottom Water (AABW) formation (B) box from that which flows north in

the Antarctic surface (A) box to allow for higher nutrient concentrations in AABW[17]. We selected these divisions to optimize the model's representation of the modern distribution of preformed nutrients and export production. However, combining either the B and A boxes or the S and T boxes does not change our results significantly.

Deep waters that upwell along the Antarctic Divergence, mix with surface waters, and then flow north are generally thought to sink again at the APF as part of the low-salinity Antarctic Intermediate Water (AAIW)[18]. Although there is considerable uncertainty[19,20], it appears that some of this recent deep water remains near the surface north of the APF where it convectively mixes with surface waters of low-latitude origin before sinking. To investigate model sensitivities to uncertainties in the fate of northward-flowing Antarctic surface waters, we allow for surface exposure of an adjustable fraction (F_a) of these waters in the subantarctic (SA) box.

After prescribing temperatures, salinities, water transports, and surface nutrients, and parametrizing the effects of biological production, air–sea gas exchange, and carbonate sediment interaction, we integrate the model to calculate the steady-state distribution of total CO_2 (ΣCO_2), the ^{13}C/^{12}C ratio ($\delta^{13}C$), total alkalinity (TA), dissolved O_2, and the atmospheric CO_2 concentration. Figure 1 depicts a solution to this model using input parameters representing the modern pre-industrial state. To assess the sensitivity of our model to variations in Antarctic ice cover, we have calculated
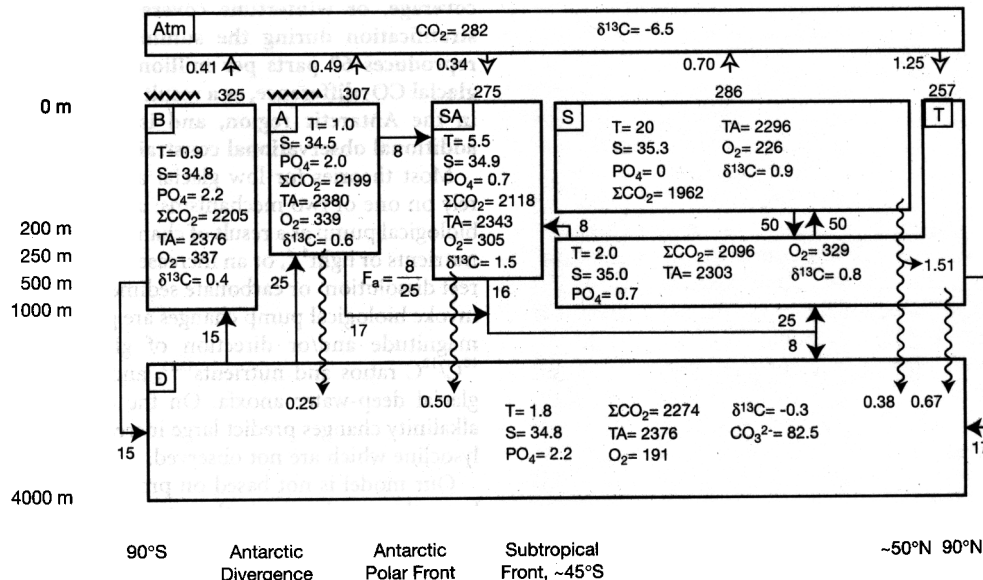

Figure 1 Solution from our atmosphere–ocean model for a best-guess modern-preindustrial state. In this state, $F_a = 0.3$, where F_a is the fraction of northward-flowing Antarctic surface waters exposed to the surface in the subantarctic (SA) box. This model consists of an atmosphere and six ocean boxes: a main surface box (S) representing the upper 200 m of water between approximately 50 °N and the Southern Subtropical Front (STF), a main thermocline box (T) representing waters between 200 and 1,000 m depth with a surface outcrop north of the main surface box, an Antarctic Bottom Water formation box (B) representing the upper 1,000 m of water south of the Antarctic Divergence (AD) ($\sim 65°$ S today), an Antarctic surface box (A) representing the upper 250 m of the Southern Ocean south of the APF ($\sim 55°$ S today) and north of the AD, a subantarctic box (SA) representing the upper 500 m of water north of the APF and south of the STF, and a deep box (D) representing the remainder of the world's oceans. Solid straight arrows denote water fluxes and are labelled in Sv. Solid wavy arrows indicate sinking fluxes of organic material and hollow arrows indicate air–sea CO_2 fluxes, and both are labelled in Gt C yr^{-1}. Numbers above the surface boxes denote CO_2 partial pressures in μatm. Values for PO$_4$, ΣCO_2, TA, dissolved O_2, and CO$_3^{2-}$ are indicated in μmol kg^{-1}, $\delta^{13}C$ in per mil, temperature T in °C, salinity S in p.s.u., and atmospheric CO_2 in p.p.m. We assume that 50% of the modern-preindustrial ocean in boxes B and A is covered by sea-ice

(represented by jagged lines), leaving a combined area of 1.6×10^{13} m^2 open for the ventilation of upwelled deep waters. We prescribe surface phosphate concentrations in the A, SA, S and T boxes, and the total ocean phosphate concentration, such that the model reproduces the observed deep preformed phosphate (PO$_4^0$) concentration of 1.4 μmol kg^{-1} and the PO$_4^0$ concentration of intermediate waters penetrating the deep ocean, also equal to 1.4 μmol kg^{-1}(ref. 30). The model consumes excess phosphate in these four surface boxes at revised Redfield proportions of -175 O$_2$:127 C:16 N:1 P. As the resulting organic matter sinks, 80% of the main surface flux is oxidized in the thermocline box and the remainder of all three fluxes in the deep box. We assume inorganic to organic carbon production ratios of 0, 1:20, 1:10 and 1:3 in the A, SA, S and T boxes respectively. The model remineralizes all sinking calcium carbonate in the deep box. We calculate fluxes across the air–sea interface assuming a perfectly mixed atmosphere and using CO_2 invasion rates of 0.15 (B, A, SA, T) and 0.05 (S) mol m^{-2} yr^{-1} μatm^{-1}, and O$_2$ gas transfer velocities of 45 (B, A, SA, T) and 15 (S) cm h^{-1}. We maintain a constant CO$_3^{2-}$ concentration in the deep box by dissolving or precipitating an appropriate amount of CaCO$_3$ (ref. 8). We have adjusted the mixing between the thermocline and surface boxes to produce a reasonable partitioning of biological productivity between these boxes.

steady-state solutions using these parameters and varying the ice-free surface area south of the APF from 1.6×10^{13} m^2 down to zero. Figure 2a shows the atmospheric CO_2 concentration for these solutions for four cases with different values of F_a.

The decrease in atmospheric CO_2 of 67 parts per million (p.p.m.) for the best-guess conditions shown in Fig. 2 is associated with a 92% decrease in the sea–to–air CO_2 flux south of the APF, and a 1.8% increase in the deep ΣCO_2 concentration, with no change in the nutrient distribution. The deep ΣCO_2 increase contributes to the dissolution of 2.5×10^{16} mol of $CaCO_3$, which produces a 1.6% increase in whole ocean alkalinity and contributes 13 p.p.m. of the total atmospheric CO_2 effect. Although not enough to produce large changes in glacial lysocline depths, this alkalinity–ice relationship is consistent with observations of a global carbonate-sediment preservation spike during deglaciation[21].

In contrast to atmospheric CO_2, the modelled deep O_2 concentration is not sensitive to ice coverage except when the outcrop area becomes very small (Fig. 2b). The change in deep O_2 from a modern-preindustrial estimate of 191 μmol kg^{-1} to a possible glacial value of 123 μmol kg^{-1} (Fig. 2b) would not produce deep anoxia. Our model also supports earlier suggestions[12,22] that sea ice is an important influence on glacial Antarctic surface $\delta^{13}C$ values. Fractionation effects associated with both net and gross air–sea CO_2 fluxes work to make the Antarctic surface box richer in ^{13}C. As these fluxes decrease with increasing ice cover, the Antarctic surface $\delta^{13}C$ value decreases by 0.7‰ (Fig. 2b). This decrease is similar to that inferred from measurements on planktonic foraminifera[12], and is in contrast to the increases in Antarctic surface $\delta^{13}C$ implied by models that invoke increases in high-latitude nutrient utilization or decreases in high-latitude vertical mixing.

Atmospheric $\delta^{13}C$ increases with increasing sea ice by 0.9‰ in the best-case model scenario. If we include an input of 500 gigatons of terrestrial carbon[23], and reduce surface temperatures by a maximum of 5 °C (ref. 24) and less in boxes that are already near the freezing point—the atmospheric $\delta^{13}C$ value returns to within 0.1‰ of the modern-preindustrial value. Measurements[15,25] indicate a sharp dip in atmospheric $\delta^{13}C$ of ~ 0.5‰ at the start of termination I, followed by a more gradual increase to a pre-industrial value several tenths of a per mil above that at the Last Glacial Maximum (LGM). Although our model does not reproduce this overall shift, it does suggest that the temporal behaviour of atmospheric $\delta^{13}C$ during deglaciation could be explained by an initial meltback of Antarctic sea ice followed by a more gradual growth in terrestrial biomass and increase in surface temperatures.

Although it is difficult to estimate the extent of glacial Antarctic sea ice, suggestions from sediment proxies of significantly increased coverage justify the investigation of its potential implications for atmospheric CO_2. There is solid evidence from ice-rafted volcanic detritus[26], and support from fossil plankton assemblages[27], that wintertime Antarctic sea ice extended to or beyond the modern APF during the LGM. However, summertime LGM ice limits are not as well constrained. Early estimates of significantly increased coverage based on sediment types[26] have been countered by recent planktonic analyses that suggest summertime Antarctic sea ice at the LGM may not have been much more extensive than today[27]. For our purposes, we expect the winter ice extent to have the main effect on deep-water ventilation, as stratification and biological productivity during summer independently limit the outgassing of CO_2 and uptake of O_2. François et al.[28] used sediment $\delta^{15}N$ and opal data to estimate that increased stratification south of the APF during glacial times led to a 70% utilization of nutrients. This would be sufficient to remove 196 μmol C kg^{-1} (0.7 $\times$ 127 $\times$ 2.2 μmol phosphate per kg) from the Antarctic surface waters, and thus prevent summertime CO_2 outgassing in our model. Furthermore, the extreme reduction in vertical mixing implied by the tenfold decrease in nutrient inputs estimated by François et al.[28] suggests that a large amount of ice remained in this region throughout the summer.

The results shown in Fig. 2 should be viewed as an indication of a potentially important mechanism in the ocean–atmosphere carbon system, rather than as an absolute prediction of the magnitude of the Antarctic sea-ice effect. However, we note that its magnitude is fairly robust with respect to variations in the assumed parameters. In addition to the sensitivities to ice-free area and F_a shown in Fig. 2a, the best-guess CO_2 difference changes by only -9 p.p.m. or $+10$ p.p.m. if the entrainment of low-latitude waters in AAIW is respectively doubled or reduced to zero. Although our model illustrates the behaviour of the ocean in the limit of no low-latitude deep-water upwelling, it is likely that there is some finite amount of diapycnal flow through the main thermocline in the real ocean. However, if we include a high-latitude sinking, low-latitude upwelling term of 10 Sv in our model, the total atmospheric CO_2 difference decreases by only 8 p.p.m. to a total of 59 p.p.m.

In addition, we have not tried to simulate increases in nutrient utilization in the subantarctic, yet in our model such changes could significantly affect the amount of CO_2 entering the deep ocean. If we reduce subantarctic surface nutrients after increasing Antarctic sea ice to generate an increase from 1.5 to 2.8 mol C m^{-2} yr^{-1} in subantarctic export production (slightly less than that proposed by François et al.[28]), the CO_2 drawdown increases by 15 p.p.m. to a total of 82 p.p.m. A final perturbation to consider is that of temperature-driven solubility changes. After reducing surface temperatures as described above, our model predicts an additional CO_2 drawdown of 27 p.p.m., corresponding to a Harvardton Bear Index[23] of 0.2. The combined effects of ice cover, subantarctic productivity, and temperature simulated by our model are
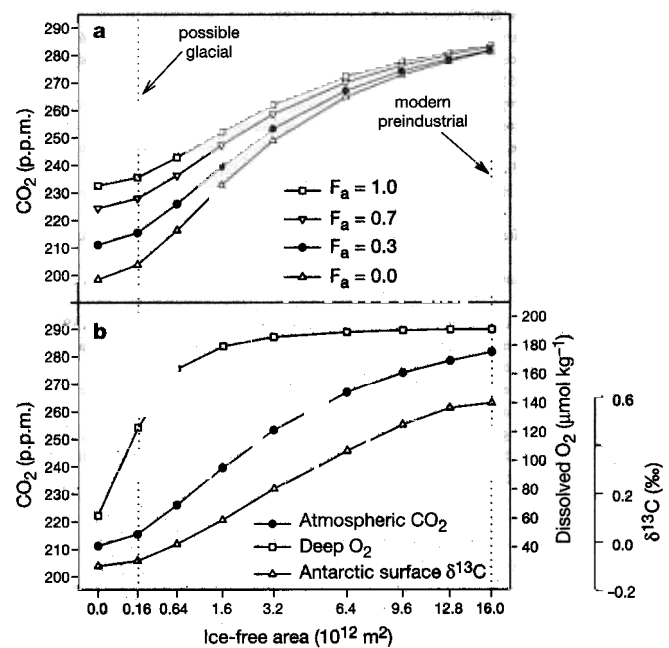

Figure 2 Steady-state model solutions for different ice coverages south of the Antarctic Polar Front (APF). We vary the exposed sea surface in the B and A boxes such that the same fraction of total surface is ice-free in each. The x-axis values represent the sum of exposed area in these two boxes, and are scaled by their square root to expand the left side of the plot. We use 1.6×10^{13} m^2 as a modern estimate of the ice-free area south of the APF, and 1.6×10^{11} m^2 to illustrate a possible glacial value. **a**, Atmospheric CO_2 using modern-preindustrial parameters and different fractions (F_a) of Antarctic surface waters entering the subantarctic box. Based on the evidence of Molinelli[19] showing the importance of subsurface transport of Antarctic waters relative to vertical mixing as the subantarctic source of AAIW, we have chosen a relatively low F_a value of 0.3 to use as a best-guess case. **b**, Atmospheric CO_2, deep O_2, and Antarctic surface $\delta^{13}C$ using $F_a = 0.3$.

sufficiently large to ensure that an 80 p.p.m. decrease in glacial atmospheric CO_2 can still be attained even after including the counteracting effects of terrestrial biomass changes and salinity-driven solubility effects[23]. Toggweiler[29] recently developed a model that similarly invokes a reduction in deep-water ventilation to explain the low glacial CO_2 levels. Whereas he generates reduced ventilation by decreasing the vertical exchange between deep and Antarctic surface waters, we suggest that reduced ventilation was driven by limitations to air–sea gas exchange imposed by increased sea ice in this region. ☐

1. Petit, J. R. et al. Climate and atmospheric history of the past 420,000 years from the Vostok ice core, Antarctica. Nature 399, 429–436 (1999).
2. Sarmiento, J. L. & Toggweiler, J. R. A new model for the role of the oceans in determining atmospheric pCO_2. Nature 308, 621–624 (1984).
3. Siegenthaler, U. & Wenk, T. Rapid atmospheric CO_2 variations and ocean circulation. Nature 308, 624–626 (1984).
4. Knox, F. & McElroy, M. B. Changes in atmospheric CO_2: Influence of the marine biota at high latitude. J. Geophys. Res. 89, 4629–4637 (1984).
5. Martin, J. H. Glacial–interglacial CO_2 change: The iron hypothesis. Paleoceanography 5, 1–13 (1990).
6. Broecker, W. S. & Henderson, G. M. The sequence of events surrounding Termination II and their implications for the cause of glacial–interglacial CO_2 changes. Paleoceanography 13, 352–364 (1998).
7. Opdyke, B. N. & Walker, J. C. G. Return of the coral reef hypothesis: Basin to shelf partitioning of $CaCO_3$ and its effect on atmospheric CO_2. Geology 20, 733–736 (1982).
8. Boyle, E. A. The role of vertical chemical fractionation in controlling Late Quaternary atmospheric carbon dioxide. J. Geophys. Res. 93, 15701–15714 (1988).
9. Archer, D. & Maier–Reimer, E. Effect of deep-sea sedimentary calcite preservation on atmospheric CO_2 concentration. Nature 367, 260–263 (1994).
10. Toggweiler, J. R. & Samuels, B. in The Global Carbon Cycle (ed. Heimann, M.) 333–366 (Springer, Berlin, 1993).
11. Gnanadesikan, A. & Toggweiler, J. R. Constraints placed by silicon cycling on vertical exchange in general circulation models. Geophys. Res. Lett. 26, 1865–1868 (1999).
12. Charles, C. D. & Fairbanks, R. G. in Geological History of the Polar Oceans: Arctic Versus Antarctic (eds Bleil, U. & Thiede, J.,) 519–538 (Kluwer Academic, Dordrecht, 1990).
13. Boyle, E. A. Cadmium and $\delta^{13}C$ paleochemical ocean distributions during the Stage 2 glacial maximum. Annu. Rev. Earth Planet. Sci. 20, 245–287 (1992).
14. Toggweiler, J. R. & Sarmiento, J. L. in The Carbon Cycle and Atmospheric CO_2: Natural Variations Archean to Present (eds Sundquist, E. T. & Broecker, W. S.) 163–184 (American Geophysical Union, Washington DC, 1985).
15. Marino, B. M., McElroy, M. B., Salawitch, R. J. & Spaulding, W. G. Glacial-to-interglacial variations in the carbon isotopic composition of atmospheric CO_2. Nature 357, 461–466 (1992).
16. Robbins, P. E. & Toole, J. M. The dissolved silica budget as a constraint on the meridional overturning circulation of the Indian Ocean. Deep-Sea Res. 44, 879–906 (1997).
17. Broecker, W. S. et al. How much deep water is formed in the Southern Ocean? J. Geophys. Res. 103, 15833–15843 (1998).
18. Tomczak, M. & Godfrey, J. S. Regional Oceanography: An Introduction 67–87 (Pergamon, Oxford, 1994).
19. Molinelli, E. J. The Antarctic influence on Antarctic Intermediate Water. J. Mar. Res. 39, 267–293 (1981).
20. McCartney, M. S. in A Voyage of Discovery (ed. Angel, M.) 103–119 (Pergamon, Oxford, 1977).
21. Berger, W. H. Deep-sea carbonate and the deglaciation preservation spike in pteropods and foraminifera. Nature 269, 301–304 (1977).
22. Broecker, W. S. An oceanographic explanation for the apparent carbon isotope–cadmium discordancy in the glacial Antarctic? Paleoceanography 8, 137–139 (1993).
23. Broecker, W. S. & Peng, T.-H. Greenhouse Puzzles 2nd edn (Eldigio, Palisades, New York, 1998).
24. Guilderson, T. P., Fairbanks, R. G. & Rubinstone, J. L. Tropical temperature variations since 20,000 years ago: Modulating interhemispheric climate change. Science 263, 663–665 (1994).
25. Smith, H. J., Fischer, H., Wahlen, M., Mastroianni, D. & Deck, B. Dual modes of the carbon cycle since the Last Glacial Maximum. Nature 400, 248–250 (1999).
26. Cooke, D. W. & Hays, J. D. in Antarctic Geoscience: Symposium on Antarctic Geology and Geophysics (ed. Craddock, C.) 1017–1025 (University of Wisconsin Press, Madison, Wisconsin, 1982).
27. Crosta, X., Pichon, J.-J. & Burckle, L. H. Reappraisal of Antarctic seasonal sea-ice at the Last Glacial Maximum. Geophys. Res. Lett. 26, 1865–1868 (1999).
28. François, R. et al. Contribution of Southern Ocean surface-water stratification to low atmospheric CO_2 concentrations during the last glacial period. Nature 389, 929–935 (1997).
29. Toggweiler, J. R. Variation of atmospheric CO_2 by ventilation of the ocean's deepest water. Paleoceanography 14, 571–588 (1999).
30. Broecker, W. S., Takahashi, T. & Takahashi, T. Sources and flow patterns of deep-ocean waters as deduced from potential temperature, salinity, and initial phosphate concentration. J. Geophys. Res. 90, 6925–6939 (1985).

Correspondence and requests for materials should be addressed to B.B.S. at the University of Colorado at Boulder (e-mail: britt@cmdl.noaa.gov).